Scientific Report

SOURCE DATA | TRANSPARENT PROCESS | OPEN ACCESS

EMBO reports

Single muscle fiber proteomics reveals unexpected mitochondrial specialization

Marta Murgia[1,2,*], Nagarjuna Nagaraj[1], Atul S Deshmukh[1,3], Marlis Zeiler[1], Pasqua Cancellara[2], Irene Moretti[4], Carlo Reggiani[2], Stefano Schiaffino[4,**] & Matthias Mann[1,3,***]

Abstract

Mammalian skeletal muscles are composed of multinucleated cells termed slow or fast fibers according to their contractile and metabolic properties. Here, we developed a high-sensitivity workflow to characterize the proteome of single fibers. Analysis of segments of the same fiber by traditional and unbiased proteomics methods yielded the same subtype assignment. We discovered novel subtype-specific features, most prominently mitochondrial specialization of fiber types in substrate utilization. The fiber type-resolved proteomes can be applied to a variety of physiological and pathological conditions and illustrate the utility of single cell type analysis for dissecting proteomic heterogeneity.

Keywords exercise; metabolism; mitochondria; muscle fibers; single cell
Subject Categories Post-translational Modifications, Proteolysis & Proteomics
DOI 10.15252/embr.201439757 | Received 20 October 2014 | Revised 23 December 2014 | Accepted 9 January 2015

Introduction

Skeletal muscle makes up about 40% of human body mass and is responsible for voluntary body movements. It plays a major role in metabolic homeostasis; for example, it is the dominant tissue in insulin-dependent glucose uptake and it is the direct conveyor of the beneficial effects of exercise [1, 2]. The repertoire of motor tasks and metabolic functions is mediated by specialized muscle fibers, which are multinucleated single cells originating from myoblasts fusion. The 'slow' type 1 and the 'fast' type 2A, 2X and 2B constitute the four basic fiber types, classically identified based on the molecular properties of their myosin heavy-chain (Myh) isoforms [3] (Supplementary Fig S1A). Fast fibers have higher shortening velocity than slow fibers, increasing in the order 2A < 2X < 2B. These properties are the result of fiber type-specific structural differences in the sarcomere and sarcoplasmic reticulum as well as in calcium transients following the action potential. From the metabolic point of view, fibers are classified into slow oxidative (SO, type 1), fast oxidative glycolytic (FOG, type 2A and 2X) and fast glycolytic (FG, type 2B) types, which have different mitochondrial content [4] (Supplementary Fig S1B). Primary muscle diseases and metabolic disorders often affect, or spare, specific fiber types through largely undefined mechanisms [3]. Importantly, the structural and metabolic properties of each fiber type can be remodeled in response to hormonal and metabolic changes and by muscle activity [4–6]. The detailed protein make-up and metabolic profile of different muscle fiber types are largely unexplored but would clearly be invaluable in understanding the effects of fiber function at the molecular level.

Single fibers have already been isolated decades ago, when pioneering studies classified subtypes based on the electrophoretic mobility of different Myh isoforms as well as contractile properties [7,8]. These studies revealed metabolic heterogeneity among muscle fibers based on measurements of enzyme activities, showing the prevalence of glycolytic enzymes in type 2 and oxidative enzymes in type 1 fibers. However, each single fiber could only be used for one or very few readouts, so that a structural and metabolic definition of fiber types, and in particular a global characterization of the different type 2 fiber subpopulations, has remained largely elusive [9]. A first step toward a larger scale view of individual muscle fibers was the transcriptomic analysis of single type 1 and 2B muscle fibers [10].

Despite great advances in mass spectrometry (MS)-based proteomics in recent years, single muscle fibers have been beyond its capabilities so far, preventing fiber type-resolved studies [11,12]. Although large compared to mononuclear cells, individual muscle fibers contain very limited protein amounts—tens or hundreds of times less than typical starting amounts in proteomics projects. Most of this protein mass consists of a few highly abundant sarcomeric proteins, which limits the capability of the mass spectrometer to fragment and identify the vast majority of low abundance species. The latter has also constrained studies at the whole muscle level, which additionally have to deal with the wide heterogeneity of muscle fibers and variations in size among different fiber types

1 Department of Proteomics and Signal Transduction, Max-Planck-Institute of Biochemistry, Martinsried, Germany
2 Department of Biomedical Sciences, University of Padova, Padua, Italy
3 Department of Proteomics, The Novo Nordisk Foundation Center for Protein Research, Faculty of Health Sciences, University of Copenhagen, Copenhagen, Denmark
4 Venetian Institute of Molecular Medicine, Padua, Italy
*Corresponding author. Tel: +49 89 8578 2402; E-mail: mmurgia@biochem.mpg.de
**Corresponding author. Tel: +39 49 7923 232; E-mail: stefano.schiaffino@unipd.it
***Corresponding author. Tel: +49 89 8578 2557; E-mail: mmann@biochem.mpg.de

[13–15]. Furthermore, muscle is a complex structure containing not only muscle fibers but also connective and adipose tissue, blood vessels and nerves, with possible variations of their relative proportions in pathophysiological conditions. With these challenges in mind, we set out to apply a highly sensitive MS-based proteomic workflow to characterize the contractile and metabolic features of individual muscle fiber types as reflected in protein abundances.

Results and Discussion

Single muscle fiber analysis of fast and slow muscles by high-sensitivity shotgun proteomics

We first obtained a deep skeletal muscle proteome by processing and enzymatically digesting whole muscle homogenates by the filter-aided sample preparation (FASP) method and separating the resulting peptide mixture into 12 fractions by isoelectric focusing [16,17]. To maximize peptide detection in order to target low abundant proteins, all measurements were performed in a linear quadrupole Orbitrap mass analyzer, characterized by high sensitivity, sequencing speed and mass accuracy [18]. This procedure yielded the quantification of about 6,500 proteins, displaying a prevalence of sarcomeric elements among the most abundant proteins and a specific enrichment in mitochondrial annotations (Supplementary Fig S2A and B). We then developed a workflow for single muscle fiber proteome analysis on the basis of a recent method, in which all preparation steps subsequent to mechanical disruption are performed in a single vessel, thereby minimizing sample loss (Fig 1A and Supplementary Methods section) [19]. We next employed the 'match between runs' feature of the MaxQuant analysis software [20]. It uses sophisticated liquid chromatography (LC) retention time alignments and precise masses to transfer peptide identifications from the deep muscle proteome, where a given peptide is much more likely to have been fragmented, to a single fiber, where often only the intact peptide has been measured (Fig 1A).

Combining the deep muscle proteome with the fiber proteome led to the quantification of a total of 7,174 proteins. Figure 1B shows the intensity signal of all proteins detected in the individual muscle fibers, ranked from the highest to the lowest abundant. The first five sarcomeric proteins account for over 50% of total signal, with myosin heavy chain ranking highest. Proteins from all other muscle compartments, including abundant proteins such as the mitochondrial ATP synthase and the sarcoplasmic reticulum (SR) calcium ATPase, are confined to the lower half of the MS-signal range. Even some transcriptional regulators, such as p65 RelA, could be identified in muscle fibers. Importantly, our data display ample coverage of metabolic features and of the mitochondrial proteome (Fig 1C), enabling us to explore the main elements of muscle metabolism at the single cell level.

Unbiased proteomics can assign fiber types and group them by function

The four major fiber types are present in the limb and trunk muscles of adult mice and were sampled in our dissection of soleus and *extensor digitorum longus* (EDL) muscles (Supplementary Fig S1A and B). Mouse muscle fibers are several mm long, and our isolation procedure typically captured 50% of a single fiber. Myh isoforms have more than 80% sequence identity; therefore, to reproduce the Myh isoform-based fiber type assignment by MS, we used only the intensities of peptides unique for each isoform for protein quantification. The relative abundance of Myh isoforms calculated from these data and the assignment of each fiber to its type is shown in Supplementary Table S1. Interestingly, in addition to the main one, virtually all of the single fibers express two or more Myh isoforms at low levels. Type 2A and 2X fibers tend to have a higher degree of heterogeneity than type 1 and 2B. Fibers containing over 80% of Myh7 (type 1) or Myh4 (2B) and over 60% of Myh1 (2X) or Myh2 (2A) were defined as pure type based on the observed average isoform expression (see Supplementary Methods and Supplementary Fig S1C). Figure 2A shows the Myh composition of two representative pure fibers per type, next to four examples of mixed-type fibers containing two or more comparably abundant isoforms.

To verify the reproducibility of MS-based fiber type assignment, we performed technical replicates by reanalyzing the peptide mixture resulting from the same single fiber. We also performed experiments in which we split the lysate from a single fiber and processed them separately. In both approaches, we arrived at essentially identical Myh compositions and always assigned the same fiber types (Supplementary Fig S3A).

Protein epitope signature tags (PrESTs) are recombinant proteins consisting of a short (generally 100–150 aa) sequence chosen from a unique region of the target proteins and a quantification tag, which can accurately quantify absolute amounts of proteins [21]. We constructed PrESTs against the different Myh isoforms and determined their absolute levels in single fibers. These ranged from undetectable to more than 500 ng per fiber. The relative isoform contributions determined from the absolute amounts were essentially superimposable on those of the relative quantification (Supplementary Fig S3B).

To investigate whether the MS-based fiber type assignment matches the traditional method based on electrophoretic properties of different Myh isoforms, we split the same fiber lysates into two parts. Half of the SDS solubilized lysate was then used to typify the fiber by an electrophoretic procedure that allows separations of Myh isoforms, whereas the other half was processed for shotgun proteomics with an in-gel-based workflow (Supplementary Methods). Again, the two methods resulted in the same Myh isoform-based fiber type classification (Fig 2B).

For estimating protein quantities for the entire detected proteome, we normalized the summed signal of the peptides identifying each protein based on protein length and peptide number (Supplementary Methods). To minimize quantitative differences among fibers due to heterogeneity in the analyzed fiber segment as a result of the isolation procedure, we normalized the entire proteome of each single fiber by the intensity of skeletal alpha actin (Acta1). The proteomes of a total of 48 pure fibers, as defined above, and assigned to fiber type by MS as described above, were used in the subsequent analyses.

To determine whether the total proteome could also assign single fibers to their correct subtypes, we performed principal component analysis (PCA). This showed a diagonal separation in the first two components of the fast-2B fibers (Fig 2C top). The intermediate position was occupied by 2A and 2X fibers, with occasional

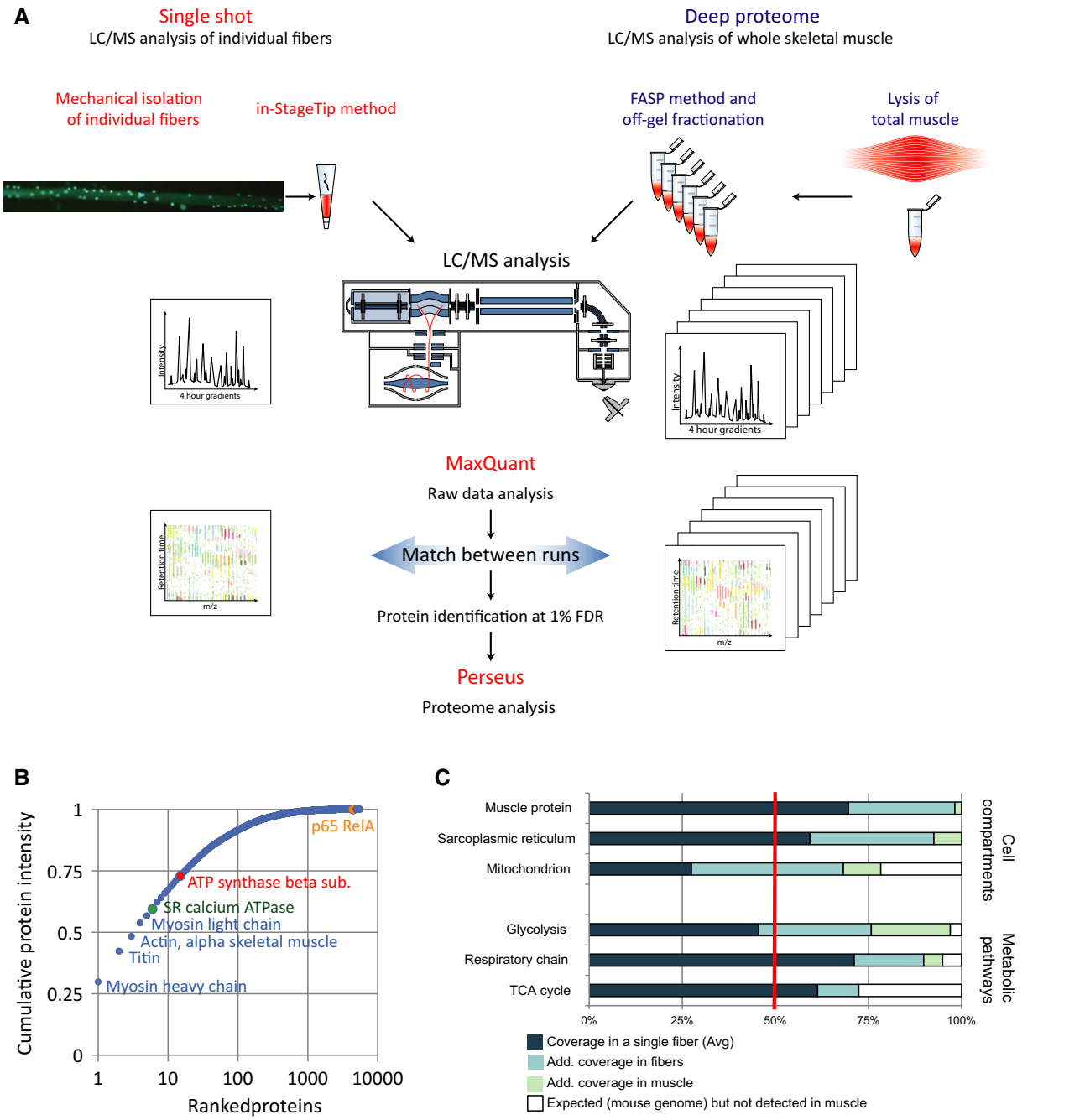

Figure 1. Characterization of the proteome of muscle fibers from fast and slow muscles.

A Shotgun proteomics workflow for fibers and whole muscle fractions. For details see main text and Materials and Methods.

B Cumulative abundance of all proteins detected in muscle fibers, ranked on a log10 scale.

C Protein coverage in muscle fibers and whole muscle. Each bar represents a selected category of keyword annotations, for which the number of corresponding protein coding genes in the mouse genome is considered as 100%. Proteins identified in our fiber database correspond to dark and light blue bars combined and additional protein identified in our whole muscle database to light green.

overlapping between groups. The corresponding 'loadings'—the main proteins driving the separation—included known fiber type-specific isoforms of sarcomeric proteins and metabolic enzymes (Fig 2C bottom).

We performed an unsupervised hierarchical clustering to verify the functional significance of the proteomic differences arising from our analysis. Unsupervised hierarchical clustering of single-fiber proteomes revealed a major cluster with high enrichment in mitochondrial annotations, spanning type 1, 2A and 2X fibers. Conversely, structural elements of excitation–contraction coupling and glycolysis defined a cluster highly intense in 2B fibers (Supplementary Fig S3C). Type 1 and 2B fibers clearly separated to the

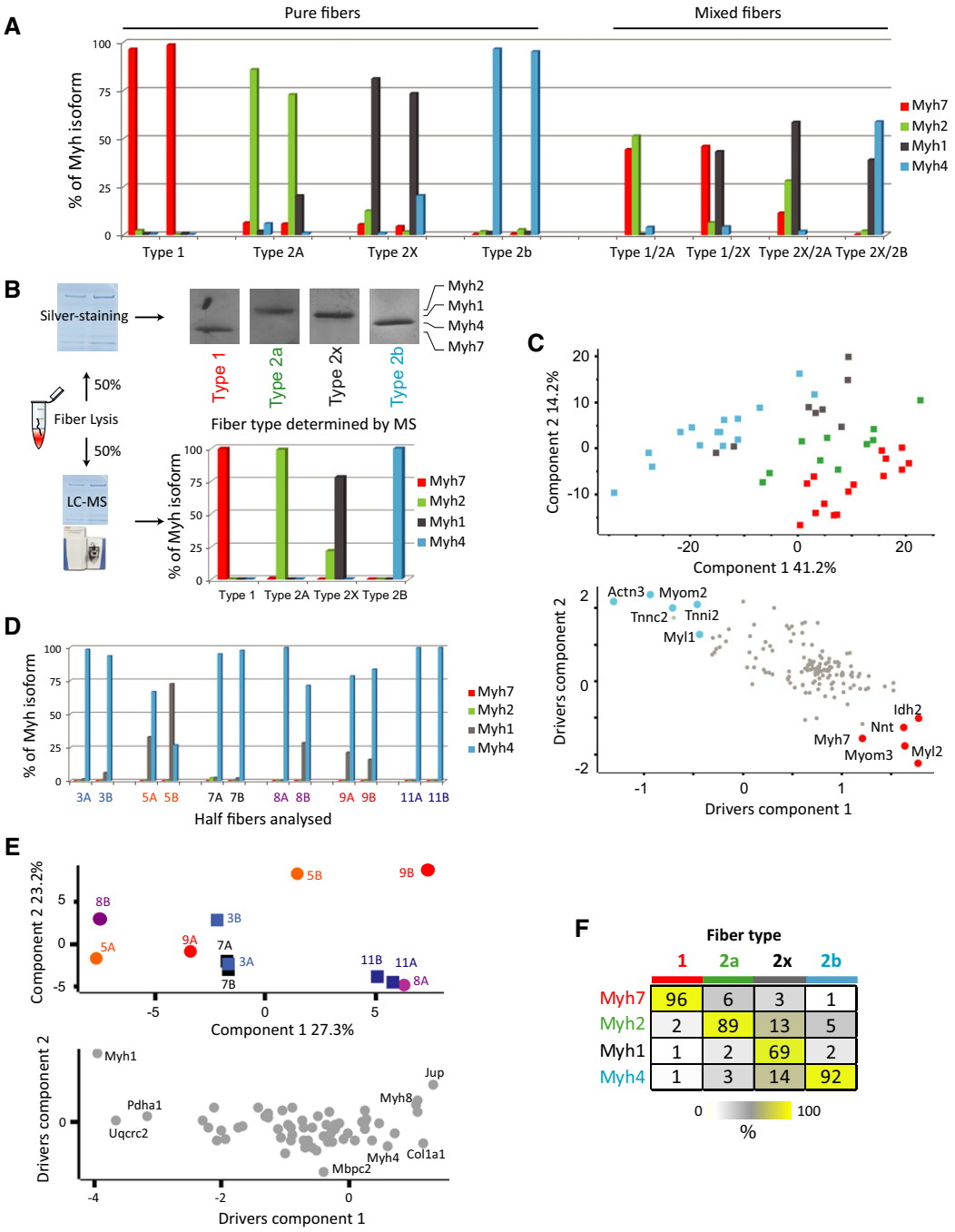

Figure 2. Fiber type assigned on the basis of Myh isoforms corresponds to specific patterns at the whole proteome level.

A MS-based quantification of Myh isoforms reveals four basic pure-type fibers and different combinations of mixed-type fibers.

B Comparison of fiber type assignment using unbiased MS-based quantification and traditional method. Fiber lysates were split into two and processed in parallel on separate gels (see Supplementary Methods). MS and Myh silver staining of the corresponding half fibers.

C Top, principal component analysis performed on pure fibers (N = 48), using only proteins expressed in all fibers; bottom, loadings showing the main proteins driving segregation into components.

D Half fibers from EDL mechanically cut at isolation and processed separately may express a very similar pattern of Myh expression (fibers 7 and 11) or a different one (fibers 3 and 8). Colors match the PCA in (E).

E Principal component analysis showing association or segregation of half-fiber proteomes. Half fibers are marked by a square if similar and by a dot if different. Samples were filtered for 100% valid values. The main proteins driving segregation into components are indicated in the bottom part of the panel. The components scale is multiplied by 10 to magnify differences.

F Distribution of Myh expression in the fiber type-resolved proteome. Values represent the enrichment in Myh isoforms as percent, calculated on the median of each fiber type and color-coded according to the scale shown at the bottom.

extremes of the heat map, whereas 2A and 2X formed intermediate mixed groups with graded properties. Thus, distinct groups of fibers can be distinguished at the total proteome level on the basis of predicted functional features.

We asked whether MS-based proteomics could reveal potential subcellular changes in Myh composition along the longitudinal fiber axis, which is a common feature in extraocular muscles [22] but has not been extensively investigated in other body muscles. Furthermore, we asked whether regional differences in Myh isoforms are associated with other segmental differences in muscle phenotype. To this end, we analyzed biological replicates, consisting of single fibers from EDL mechanically cut into two halves directly after isolation. Myh isoform analysis and PCA revealed that biological replicates were in general more different than technical replicates (Fig 2D, see Supplementary Fig S3A for comparison) and were in some cases quite distinct at the proteome level (Fig 2D and E, Supplementary Fig S3D). Our observation at the proteome scale is in accord with previous reports in rabbit limb muscles, of nonuniform distribution of fast- and slow-myosin subunits along the axis of single fibers [23]. Regional changes can be profound in some cases, which is in agreement with pioneering physiological studies showing segmental differences in the shortening velocity of single fibers [24]. These results also indicate that proteomics can now quantify biological heterogeneity within a single cellular unit.

Our precise and unbiased fiber type assignment allows us to define a fiber type-resolved proteome: We assign each single and pure fiber to its proper subtype and obtain the median estimated expression values of each protein in the subtype (Supplementary Table S2). Figure 2F shows that each of the subset proteomes has the expected distribution of fiber type-specific Myh isoforms, validating this procedure.

Differences in structural proteins between subtypes

The single-fiber-resolved proteomes for the first time afford a global view of the fiber type distribution of contractile and cytoskeletal protein isoforms and can be inspected in the MaxQB database [25]. The data support many previous observations, for instance high expression levels of Actn3 in 2B fibers, but also reveal novel features. An example is the fourfold higher expression of Tcap/telethonin in type 1 than in fast fibers, a finding which we verified by Western blotting (Supplementary Fig S4A and B).

Most protein components of the sarcoplasmic reticulum and T-tubule system show a higher abundance in type 2B fibers (Supplementary Fig S4C), as expected from the greater development of these membrane systems in fast fibers [26]. A novel finding is that the T-tubule protein STAC3, involved in excitation–contraction coupling, is about fourfold more abundant in 2B and 2X compared to type 1 and 2A fibers. This is likely the result of post-translational regulation, since qPCR analysis did not reveal any significant difference between fast and slow muscles [27]. Atlastin 2 (Atl2) and Lunapark (Lnp) have opposite roles in generating and maintaining the shape of the endoplasmic/sarcoplasmic reticulum, and specifically in either promoting tubule formation and branching (Atl2) or inhibiting branching (Lnp) [28,29]. Our data document their presence in muscle fibers and reveal that Atl2 is twofold more abundant in 2B and 2X fibers, which have a more convoluted SR, whereas Lnp is threefold more abundant in type 1, 2A and 2X fibers, which have a less developed SR than type 2B [30].

To discover potential new fiber type-specific proteins in an unbiased manner, we designed eight expression profiles, each characterized by high expression in one of the subtypes, and searched with a correlation analysis the proteins with the most similar expression profile (Supplementary Fig S5). This analysis retrieved known or predicted subtype-specific proteins but also novel ones. For instance, Mitsugumin-53/Trim72, a protein that plays a role in membrane repair, is fivefold higher in type 1 than in all another fiber types. While the physiological significance of these observations needs to be addressed further, they illustrate the potential of our results for the discovery of new fiber type-specific features.

Fiber type-specific differences in the mitochondrial proteome

Skeletal muscle is a tissue with high energy demand and is frequently affected in mitochondrial diseases. Our single-fiber proteomes covered a total of 654 proteins annotated as mitochondrial, with an average of more than 270 quantified in individual fibers. The majority of components of the respiratory chain and TCA cycle were quantified in each fiber as well (Fig 1C). Type 2B fibers are known to have lower mitochondrial content, and this was clearly reflected in our measurements (Supplementary Table S2). Intriguingly, however, our data now reveal that the major pathways—OXPHOS, beta-oxidation and TCA cycle—show significant variations among the various fiber types (Fig 3A). These differences imply the existence of distinct subsets of mitochondrial proteins associated with specific fiber types and are discussed below.

OXPHOS protein levels were especially abundant in 2A fibers, in accordance with the greatest content of mitochondria among the subtypes (Supplementary Fig S6) [26]. However, when we normalized for mitochondrial content (using cytochrome c or succinate dehydrogenase as indicators of mitochondrial quantity [31]), other protein subsets significantly deviated from this simple trend, therefore reflecting functional mitochondrial heterogeneity. Type 1 fibers had highest protein levels in enzymes responsible for beta-oxidation, located in the mitochondrial matrix, including Acadl, Hadha, Etfa and Etfb complex and Etfdh. After this normalization, the differences in proteins involved in beta-oxidation were statistically significant between subtypes ($P < 0.05$) (Supplementary Table S3). Proteins involved in the conversion of fatty acids to fatty acyl-CoA esters via Acsl1, located in the outer mitochondrial membrane, and proteins involved in fatty acid import at the inner mitochondrial membrane such as Cpt2A were similarly prevalent in type 1 fibers. The same held true for proteins involved in ketone body metabolism, such as Oxct1, an enzyme responsible for acetoacetyl-CoA production from acetoacetate, and Acat1, which converts acetoacetyl-CoA into acetyl-CoA (Fig 3A and Supplementary Table S3).

Proteins associated with the regulation of pyruvate dehydrogenase (PDH) and the TCA cycle show greater abundance in type 2X fibers. For example, the protein phosphatase Pdp1 is more than twofold more abundant than in other subtypes. When muscle fibers are stimulated by insulin or by contractile activity, Pdp1 dephosphorylates the E1α subunit of PDH, thus activating the PDH complex. Relatively high concentration of Pdp1 in type 2X fibers may

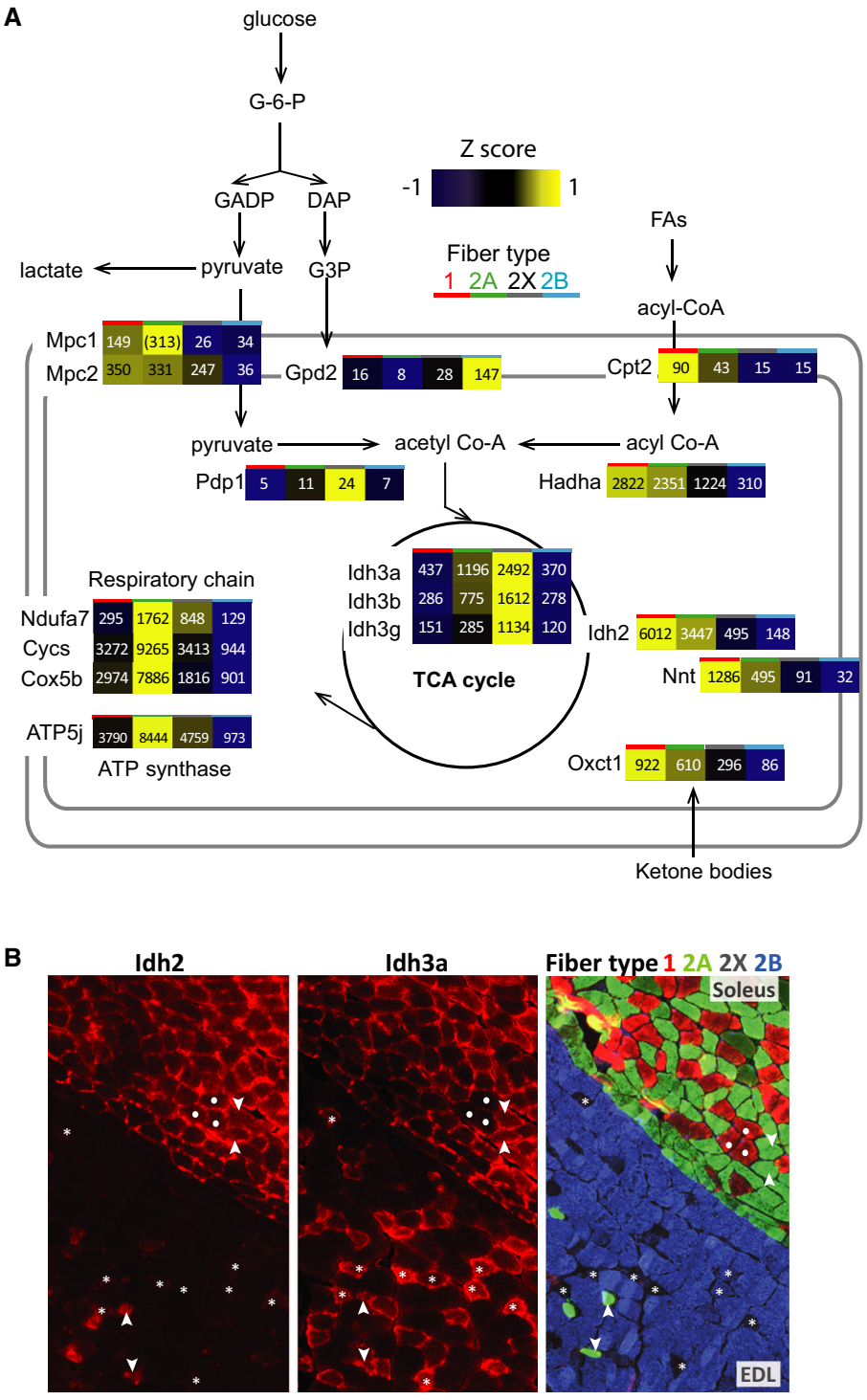

Figure 3. Fiber type-resolved features of muscle metabolism.

A Differential distribution of selected mitochondrial proteins or pathways according to muscle fiber type. The normalized expression (by actin) of each protein in different fiber types is reported; the color scale is based on Z-score as indicated. Boxes represent the values of each fiber type, always following the order type 1/2A/2X/2B from left to right, as indicated on top. Proteins are identified by the corresponding gene name (see also Supplementary Table S2 for reference). Brackets indicate less than 3 valid values in one group.

B Differential distribution of Idh3 and Idh2 in fiber types validated by immunohistochemistry in serial sections of soleus and EDL muscles. Fiber type distribution is shown in the right panel using a combination of antibodies specific to Myh isoforms; pseudocolors have been adjusted to match the fiber type color coding used throughout the paper. Representative type 1 (dot), 2A (arrowhead) and 2X (asterisk) are indicated.

Source data are available online for this figure.

better prepare these fibers to activate PDH activity and thus the TCA cycle in response to stimulation. The NAD-dependent isocitrate dehydrogenase 3 (Idh3) is a member of the TCA cycle, and all three different subunits of this heterotetramer are likewise more than twofold higher (Fig 3A). Isocitrate dehydrogenase activity was previously reported to be higher in mitochondria isolated from fast glycolytic, type 2B muscles [32, 33]. However, 2B fibers could not be distinguished from 2X fibers in those studies, whereas our data clearly show that Idh3 is higher in type 2X fibers whereas it is lowest in 2B fibers. To confirm these findings with an independent approach, we stained serial sections of soleus and EDL with antibodies specific to Idh3a and assigned fiber type using Myh isoform-specific antibodies (Fig 3B, left). In accord with our MS results, Idh3 showed a reactivity largely corresponding to type 2X fibers (asterisk) in EDL and was higher in type 2A than in type 1 fibers (dot) in soleus. Other TCA cycle enzymes, such as malate dehydrogenase (Mdh2), were also significantly more highly expressed in 2X fibers (Supplementary Table S3). Interestingly, TCA cycle genes were the most abundant mitochondrial genes induced by the overexpression of the transcriptional coactivator PGC-1beta, which was reported to selectively drive the formation of type 2X fibers in skeletal muscle [34].

Another mitochondrial isocitrate dehydrogenase isoform, Idh2, caught our attention because its expression levels were reversed compared to Idh3, with dramatically higher expression levels in type 1 fibers (> 30-fold difference between type 1 and 2B). Indeed, we confirmed by immunohistochemistry (Fig 3B, middle panel) that Idh2 was highly expressed in soleus, with only occasional small fibers in EDL corresponding to type 2A fibers (arrowheads). Idh2 is a NADP-dependent enzyme that is structurally different from Idh3, whose functional role is the object of debate. According to one interpretation, Idh2 does not contribute to flux through the TCA cycle like Idh3 but actually works in the reverse direction, converting glutamine-derived alpha-ketoglutarate into citrate, a source of carbon for fatty acid synthesis [35]. An alternative interpretation is based on the observation that individuals homozygous for loss-of-function mutations in *IDH3B*, encoding the β subunit of Idh3, show no alteration associated with the corresponding enzyme deficiency in any tissue except for the retina [36]. Idh2 activity was normal in affected individuals, suggesting that Idh2 can act like Idh3 in the isocitrate to α-ketoglutarate forward reaction of the TCA cycle. Our data show that type 1 fibers, which have abundant Idh2 protein levels, contain relatively low amounts of Idh3 subunits, comparable to those present in the mitochondria-poor type 2B fibers. This supports the notion that Idh2 is the major TCA cycle enzyme responsible for the oxidative decarboxylation of isocitrate in slow type 1 fibers.

Nicotinamide nucleotide transhydrogenase (Nnt), located in the mitochondrial inner membrane, can also produce NADPH like Idh2. Interestingly, the relative distribution of Nnt protein matches that of Idh2 (> 30-fold difference between type 1 and 2B) (Fig 3). NADPH generated by Idh2 or Nnt can be used for the reduction of glutathione and thioredoxins counteracting reactive oxygen species (ROS), which are presumably higher in mitochondria from type 1 fibers due to the more active fatty acid beta-oxidation pathway [37]. Thus, the heterogeneity in the TCA cycle between subtypes discovered by single-fiber proteomics can shed new light on differential substrate utilization.

Another striking observation was that Gpd2, the mitochondrial component of the glycerophosphate shuttle, was about tenfold more abundant in type 2B fibers, even though they have the lowest mitochondrial content. Other proteins have a significantly higher expression in 2B fibers after normalization for mitochondrial content (Supplementary Table S4). A previous study had already reported higher levels of Gpd2 in type 2B fibers [33]. This finding suggests that a significant portion of glycolytic flux in 2B fibers is diverted to the formation of the glycerol 3-phosphate that shuttles to mitochondria where it is transformed into dihydroxyacetone phosphate by Gpd2 activity. The glycerophosphate shuttle contributes to the reoxidation of cytosolic NADH produced by glycolysis, thus enabling a sustained ATP production by the glycolytic pathway without excessive accumulation of lactic acid [38]. Conversely, our proteomics data indicate that the capacity for mitochondrial import of pyruvate is limited in 2B fibers because of the more than fivefold lower protein levels of the mitochondrial pyruvate carrier, which is formed by two recently discovered small proteins, Mpc1 and Mpc2, located in the mitochondrial inner membrane [39, 40]. The distribution of Mpc1 and Mpc2 in skeletal muscle fibers has not been previously investigated, and their stoichiometry in the complex is not known. Here, we observe significant variations in the ratio of the two subunits in different fiber types, with Mpc2 abundant in type 1, 2A and 2X fibers, whereas Mpc1 has higher levels in type 1 compared to 2X and 2B fibers.

Previous biochemical studies in single muscle fibers, such as the seminal studies by Lowry [7] and Pette [41], have revealed the existence of a wide range of activity for a number of mitochondrial enzymes, with the tendency for slow type 1 fibers showing highest activities, fast glycolytic 2B fibers lowest activities and type 2A fibers intermediate activities. The interpretation was that those differences reflected essentially quantitative differences in the amount of mitochondria and oxidative enzyme along a continuous spectrum between the two extremes of mitochondria-rich and mitochondria-poor fibers. A limitation of those studies was that only few enzymes were analyzed and fiber typing was not precise. Our proteomic studies based on quantitative measures of hundreds of mitochondrial proteins in four fiber types reveal a more complex scenario and clearly establish that mitochondria differ in the various muscle fiber types not only quantitatively but also qualitatively, with various subsets of mitochondrial proteins showing distinct fiber type-specific patterns of metabolic function. This supports the notion of metabolic specialization that is finely tuned to the physiological properties of muscle fibers. With further streamlining of the technology, similar experiments could now be done in humans and as a function of drug, exercise or disease perturbation.

Materials and Methods

Preparation of single muscle fibers

Soleus and EDL muscles were isolated from 3-month-old wild-type CD1 mice (Charles River), housed in a standard environment with water and food *ad libitum*. The animals ($N = 10$) were sacrificed by cervical dislocation and the muscles immediately removed by cutting through the tendons. Fibers were mechanically dissociated

in an ice-cold solution containing potassium propionate (150 mM), KH_2PO_4 (5 mM), magnesium acetate (5 mM), EGTA (5 mM) and DTT (1 mM) using tweezers and individually transferred to standard Eppendorf tubes. Some fibers were cut into two halves at isolation and frozen in separate tubes. Fibers were lysed and proteolytically digested as described in Supplementary Methods.

Liquid chromatography and mass spectrometry

Peptides were separated on 50-cm columns of ReproSil-Pur C18-AQ 1.9 μm resin (Dr. Maisch GmbH) packed in-house. The columns were kept at 50°C using a custom-made column oven controlled by the SprayQC software [42]. Liquid chromatography performed on an EASY-nLC 1000 ultra-high-pressure system was coupled through a nanoelectrospray source to a Q Exactive mass spectrometer (all from Thermo Fisher Scientific). Peptides were loaded in buffer A (0.1% (v/v) formic acid) applying a nonlinear 270-min gradient of 2–60% buffer B (0.1% (v/v) formic acid, 80% (v/v) acetonitrile) at a flow rate of 250 nl/min. Data acquisition switched between a full scan and 5–10 data-dependent MS/MS scans. Multiple sequencing of peptides was minimized by excluding the selected peptide candidates for 45 s.

Computational proteomics

The MaxQuant software (version 1.4.3.19) was used for the analysis of raw files. Peak lists were searched against the mouse Uniprot FASTA database version of February 25, 2012 (81213 entries) and a common contaminants database (247 entries) by the Andromeda search engine [20, 43]. False discovery rate was set to 1% for peptides (minimum length of 7 amino acids) and proteins and was determined by searching a reverse database. A maximum of three missed cleavages were allowed in the database search. Peptide identification was performed with an allowed initial precursor mass deviation up to 7 ppm and an allowed fragment mass deviation 20 ppm. The mass spectrometry proteomics data have been deposited to the ProteomeXchange Consortium via the PRIDE partner repository with the dataset identifier PXD001641.

Bioinformatic analysis

Analyses were performed with the Perseus software (version 1.4.2.23), part of the MaxQuant environment (http://www.perseus-framework.org). Categorical annotations were supplied in the form of Uniprot Keywords, extracted from the UniProt database. Two-sample Welch tests were performed using 0.05 FDR for truncation and 250 randomizations. Protein intensity values normalized by protein length were divided by the value of skeletal actin (Acta) and then multiplied by a constant to obtain integers. We performed hierarchical clustering on *Z*-score normalized proteins. To determine enrichments in clusters, Fisher's exact test was carried out with an FDR value of 0.04.

Immunohistochemistry

Cryosections of soleus and EDL muscles, frozen as a single block, were fixed in 4% paraformaldehyde and permeabilized using 0.2% Triton X-100 prior to staining with antibodies anti-Idh2 (HPA007831) and Idh3a (AV42237), both polyclonals from SIGMA. Immunofluorescence with Myh isoform-specific antibodies was performed as described in [44].

Supplementary information for this article is available online: http://embor.embopress.org

Acknowledgements

We thank Korbinian Mayr, Igor Paron and Gabriele Sowa for their assistance with MS; Stefano Ciciliot for the pictures of muscle sections; Francesca Forner for performing pilot experiments; Nils Kulak, Stefka Tyanova, Tikira Temu, Marco Hein and Markus Raeschle for critical discussions; and the PRIDE Team for the data deposition. This work was supported by the Max-Planck Society for the Advancement of Science; The Novo Nordisk Foundation Center for Basic Metabolic Research, Copenhagen, Denmark; The Louis Jeantet Foundation; and EU 7th Framework Programme (grant agreement HEALTH-F4-2008-201648/PROSPECTS).

Author contributions

MMu, PC and CR prepared fibers; ASD produced whole muscle fractions; MZ designed and analyzed PrESTs experiments; NN wrote the MS methods; IM performed immunostainings; MMu and NN performed and evaluated MS experiments; MMu, SS, CR and MMa analyzed data; and MMu, SS, CR and MMa wrote the paper.

Conflict of interest

The authors declare that they have no conflict of interest.

References

1. Richter EA, Ruderman NB (2009) AMPK and the biochemistry of exercise: implications for human health and disease. *Biochem J* 418: 261 – 275
2. Boström P, Wu J, Jedrychowski MP, Korde A, Ye L, Lo JC, Rasbach KA, Boström EA, Choi JH, Long JZ *et al* (2012) A PGC1-alpha-dependent myokine that drives brown-fat-like development of white fat and thermogenesis. *Nature* 481: 463 – 468
3. Ciciliot S, Rossi AC, Dyar KA, Blaauw B, Schiaffino S (2013) Muscle type and fiber type specificity in muscle wasting. *Int J Biochem Cell Biol* 45: 2191 – 2199
4. Bassel-Duby R, Olson EN (2006) Signaling pathways in skeletal muscle remodeling. *Annu Rev Biochem* 75: 19 – 37
5. Baldwin KM, Haddad F, Pandorf CE, Roy RR, Edgerton VR (2013) Alterations in muscle mass and contractile phenotype in response to unloading models: role of transcriptional/pretranslational mechanisms. *Front Physiol* 4: 284
6. Egan B, Zierath JR (2013) Exercise metabolism and the molecular regulation of skeletal muscle adaptation. *Cell Metab* 17: 162 – 184
7. Lowry CV, Kimmey JS, Felder S, Chi MM, Kaiser KK, Passonneau PN, Kirk KA, Lowry OH (1978) Enzyme patterns in single human muscle fibers. *J Biol Chem* 253: 8269 – 8277
8. Luff AR, Atwood HL (1972) Membrane properties and contraction of single muscle fibers in the mouse. *Am J Physiol* 222: 1435 – 1440
9. Pette D, Peuker H, Staron RS (1999) The impact of biochemical methods for single muscle fibre analysis. *Acta Physiol Scand* 166: 261 – 277
10. Chemello F, Bean C, Cancellara P, Laveder P, Reggiani C, Lanfranchi G (2011) Microgenomic analysis in skeletal muscle: expression signatures of individual fast and slow myofibers. *PLoS ONE* 6: e16807

11. Cox J, Mann M (2011) Quantitative, high-resolution proteomics for data-driven systems biology. *Annu Rev Biochem* 80: 273 – 299
12. Altelaar AF, Heck AJ (2012) Trends in ultrasensitive proteomics. *Curr Opin Chem Biol* 16: 206 – 213
13. Ohlendieck K (2013) Proteomic identification of biomarkers of skeletal muscle disorders. *Biomark Med* 7: 169 – 186
14. Drexler HC, Ruhs A, Konzer A, Mendler L, Bruckskotten M, Looso M, Günther S, Boettger T, Krüger M, Braun T (2012) On marathons and Sprints: an integrated quantitative proteomics and transcriptomics analysis of differences between slow and fast muscle fibers. *Mol Cell Proteomics* 11: M111.010801
15. Gelfi C, Vasso M, Cerretelli P (2011) Diversity of human skeletal muscle in health and disease: contribution of proteomics. *J Proteomics* 74: 774 – 795
16. Wisniewski JR, Zougman A, Nagaraj N, Mann M (2009) Universal sample preparation method for proteome analysis. *Nat Methods* 6: 359 – 362
17. Hubner NC, Ren S, Mann M (2008) Peptide separation with immobilized pI strips is an attractive alternative to in-gel protein digestion for proteome analysis. *Proteomics* 8: 4862 – 4872
18. Michalski A, Damoc E, Hauschild JP, Lange O, Wieghaus A, Makarov A, Nagaraj N, Cox J, Mann M, Horning S (2011) Mass spectrometry-based proteomics using Q Exactive, a high-performance benchtop quadrupole Orbitrap mass spectrometer. *Mol Cell Proteomics* 10: M111.011015
19. Kulak NA, Pichler G, Paron I, Nagaraj N, Mann M (2014) Minimal, encapsulated proteomic-sample processing applied to copy-number estimation in eukaryotic cells. *Nat Methods* 11: 319 – 324
20. Cox J, Mann M (2008) MaxQuant enables high peptide identification rates, individualized p.p.b.-range mass accuracies and proteome-wide protein quantification. *Nat Biotechnol* 26: 1367 – 1372
21. Zeiler M, Straube WL, Lundberg E, Uhlen M, Mann M (2012) A Protein Epitope Signature Tag (PrEST) library allows SILAC-based absolute quantification and multiplexed determination of protein copy numbers in cell lines. *Mol Cell Proteomics* 11: O111.009613
22. Park KA, Lim J, Sohn S, Oh SY (2012) Myosin heavy chain isoform expression in human extraocular muscles: longitudinal variation and patterns of expression in global and orbital layers. *Muscle Nerve* 45: 713 – 720
23. Staron RS, Pette D (1987) Nonuniform myosin expression along single fibers of chronically stimulated and contralateral rabbit tibialis anterior muscles. *Pflugers Arch* 409: 67 – 73
24. Edman KA, Reggiani C, te Kronnie G (1985) Differences in maximum velocity of shortening along single muscle fibres of the frog. *J Physiol* 365: 147 – 163
25. Schaab C, Geiger T, Stoehr G, Cox J, Mann M (2012) Analysis of high accuracy, quantitative proteomics data in the MaxQB database. *Mol Cell Proteomics* 11: M111.014068
26. Schiaffino S, Hanzlikova V, Pierobon S (1970) Relations between structure and function in rat skeletal muscle fibers. *J Cell Biol* 47: 107 – 119
27. Nelson BR, Wu F, Liu Y, Anderson DM, McAnally J, Lin W, Cannon SC, Bassel-Duby R, Olson EN (2013) Skeletal muscle-specific T-tubule protein STAC3 mediates voltage-induced Ca2 + release and contractility. *Proc Natl Acad Sci USA* 110: 11881 – 11886
28. Voeltz GK, Prinz WA, Shibata Y, Rist JM, Rapoport TA (2006) A class of membrane proteins shaping the tubular endoplasmic reticulum. *Cell* 124: 573 – 586
29. Chen S, Novick P, Ferro-Novick S (2013) ER structure and function. *Curr Opin Cell Biol* 25: 428 – 433
30. Luff AR, Atwood HL (1971) Changes in the sarcoplasmic reticulum and transverse tubular system of fast and slow skeletal muscles of the mouse during postnatal development. *J Cell Biol* 51: 369 – 383
31. Mootha VK, Bunkenborg J, Olsen JV, Hjerrild M, Wisniewski JR, Stahl E, Bolouri MS, Ray HN, Sihag S, Kamal M *et al* (2003) Integrated analysis of protein composition, tissue diversity, and gene regulation in mouse mitochondria. *Cell* 115: 629 – 640
32. Glancy B, Balaban RS (2011) Protein composition and function of red and white skeletal muscle mitochondria. *Am J Physiol Cell Physiol* 300: C1280 – C1290
33. Jackman MR, Willis WT (1996) Characteristics of mitochondria isolated from type I and type IIb skeletal muscle. *Am J Physiol* 270: C673 – C678
34. Arany Z, Lebrasseur N, Morris C, Smith E, Yang W, Ma Y, Chin S, Spiegelman BM (2007) The transcriptional coactivator PGC-1beta drives the formation of oxidative type IIX fibers in skeletal muscle. *Cell Metab* 5: 35 – 46
35. Wise DR, Ward PS, Shay JE, Cross JR, Gruber JJ, Sachdeva UM, Platt JM, DeMatteo RG, Simon MC, Thompson CB *et al* (2011) Hypoxia promotes isocitrate dehydrogenase-dependent carboxylation of alpha-ketoglutarate to citrate to support cell growth and viability. *Proc Natl Acad Sci USA* 108: 19611 – 19616
36. Hartong DT, Dange M, McGee TL, Berson EL, Dryja TP, Colman RF (2008) Insights from retinitis pigmentosa into the roles of isocitrate dehydrogenases in the Krebs cycle. *Nat Genet* 40: 1230 – 1234
37. Speijer D (2014) How the mitochondrion was shaped by radical differences in substrates: what carnitine shuttles and uncoupling tell us about mitochondrial evolution in response to ROS. *BioEssays* 36: 634 – 643
38. Mracek T, Drahota Z, Houstek J (2013) The function and the role of the mitochondrial glycerol-3-phosphate dehydrogenase in mammalian tissues. *Biochim Biophys Acta* 1827: 401 – 410
39. Bricker DK, Taylor EB, Schell JC, Orsak T, Boutron A, Chen YC, Cox JE, Cardon CM, Van Vranken JG, Dephoure N *et al* (2012) A mitochondrial pyruvate carrier required for pyruvate uptake in yeast, Drosophila, and humans. *Science* 337: 96 – 100
40. Herzig S, Raemy E, Montessuit S, Veuthey JL, Zamboni N, Westermann B, Kunji ER, Martinou JC (2012) Identification and functional expression of the mitochondrial pyruvate carrier. *Science* 337: 93 – 96
41. Pette D, Staron RS (1990) Cellular and molecular diversities of mammalian skeletal muscle fibers. *Rev Physiol Biochem Pharmacol* 116: 1 – 76
42. Scheltema RA, Mann M (2012) SprayQc: a real-time LC-MS/MS quality monitoring system to maximize uptime using off the shelf components. *J Proteome Res* 11: 3458 – 3466
43. Cox J, Neuhauser N, Michalski A, Scheltema RA, Olsen JV, Mann M (2011) Andromeda: a peptide search engine integrated into the MaxQuant environment. *J Proteome Res* 10: 1794 – 1805
44. Dyar KA, Ciciliot S, Wright LE, Biensø RS, Malagoli Tagliazucchi G, Patel VR, Forcato M, Peña Paz MI, Gudiksen A, Solagna F *et al* (2014) Muscle insulin sensitivity and glucose metabolism are controlled by the intrinsic muscle clock. *Mol Metab* 3: 29 – 41